Journal of Oceanography, Vol. 66, pp. 41 to 60, 2010

Effects of Mass Source/Sink at the Western Boundary on the Wind-Driven Gyres: Implications for the Ventilation of the North Pacific Intermediate Layer through Convection in the Okhotsk Sea and Tidal Mixing at the Kuril Straits

Tomohiro Nakamura[1]*, Takahiro Toyoda[2], Yoichi Ishikawa[3] and Toshiyuki Awaji[3]

[1]*Pan-Okhotsk Research Center, Institute of Low Temperature Science, Hokkaido University, Sapporo 060-0819, Japan*
[2]*Ocean Climate Change Research Program, Research Institute for Global Change, JAMSTEC, Yokohama 236-0001, Japan*
[3]*Department of Geophysics, Graduate School of Science, Kyoto University, Kyoto 606-8502, Japan*

(Received 26 July 2008; in revised form 21 August 2009; accepted 21 August 2009)

A steady quasi-geostrophic 2.5-layer model, forced by both Ekman pumping and a mass source/sink situated at the western boundary has been constructed to investigate the effect of diapycnal transport due to convection in the Okhotsk Sea and tidal mixing at the Kuril Straits on the intermediate layer in the North Pacific. The model illustrates a combined effect of the wind-driven and mass-driven circulations. First, net mass input induces a "barotropic" mode inter-gyre flow along the western boundary through the dynamical influence of Kelvin waves. This flow creates characteristic curves (geostrophic contours) that facilitate inter-gyre communication through the western boundary layer from the location of the mass source to the subtropical gyre. Due to the effect of wind-driven circulation, the offshore part turns eastward into the interior, encircles the outer rim of the region (which would otherwise be the pool region in the absence of mass input), and then encounters the western boundary. Eventually, the water fed into the lower layer flows mostly along this path and later flows away to the equatorial region. Conversely, in the upper layer, water is fed from the equator to the subtropics, and to the subpolar interior region through the western boundary current. The water then circulates along the outer rim and is absorbed into the mass sink. The model is controlled mainly by three nondimensional parameters: (1) the ratio of net mass input rate to the maximum Sverdrup transport (Q/T_{Sv}^{max}), which affects the inter-gyre communication by altering the paths of geostrophic contours, (2) the ratio of a mass input rate into the lower layer to that in total (Q_2/Q), which controls the vertical structure of the inter-gyre flow, and (3) the measure of the wind forcing effect relative to the β effect, which determines the horizontal extent of the area influenced by the mass input. The other parameter regimes with respect to Q/T_{Sv}^{max} and Q_2/Q are also presented.

Keywords:
· Intermediate layer,
· unventilated thermocline theory,
· inter-gyre communication,
· North Pacific Intermediate Water,
· analytical model,
· steady quasi-geostrophic model.

1. Introduction

The intermediate layer of the North Pacific Ocean is ventilated mainly from the Okhotsk Sea (e.g., Talley, 1993; Warner *et al*., 1996; Yasuda *et al*., 1996), a body of water located to the northwest of the Pacific and separated from it by the Kuril Straits (Fig. 1). The ventilation process involves the formation of the North Pacific Intermediate Water (NPIW), which spreads over most of the subtropical gyre and intrudes into the tropics (e.g., Talley, 1993). The NPIW stores large volumes of greenhouse gases such as CO_2 (e.g., Yamanaka and Tajika, 1996) and considerable quantities of heat and fresh water. A dynamical understanding of how the water influ-

* Corresponding author. E-mail: nakamura@lowtem.hokudai.ac.jp

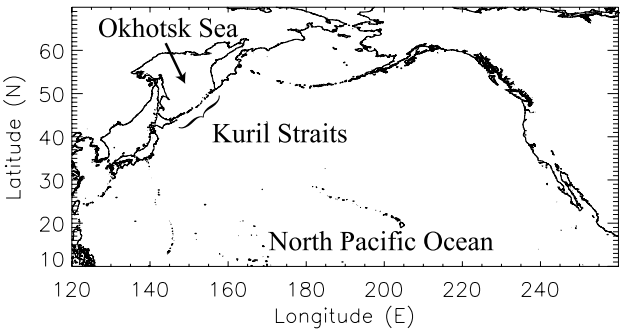

Fig. 1. Locations of the Okhotsk Sea and the Kuril Straits.

enced by ventilation circulates in the intermediate layer is important in understanding, predicting, and monitoring the potential response of the North Pacific to long-term climate variability.

In the Okhotsk Sea, the deepest convection in the North Pacific is associated with the strong, cold winter monsoon and copious sea ice production (e.g., Kitani, 1973; Alfultis and Martin, 1987; Talley, 1991). Vigorous vertical mixing is also induced in the Kuril Straits (Yasuoka, 1968; Kitani, 1973; Kawasaki and Kono, 1994; Gladyshev, 1995; Aramaki *et al*., 2001), mainly by tides (Nakamura *et al*., 2000; Nakamura and Awaji, 2001, 2004). The convection ventilates the upper part of the intermediate layer ($\lesssim 27.0\sigma_\theta$), whereas tidally induced vertical mixing is thought to be a main cause of ventilating the lower part ($27.0\sim27.6\sigma_\theta$). This is because observed distributions of Chlorofluorocarbons (CFCs) indicate that the ventilation in the North Pacific extends to much deeper, denser layers ($\sim27.6\sigma_\theta$) than the deepest convection ($\sim27.0\sigma_\theta$), and that the most recently ventilated water in such dense layers lies around the Kuril Straits (Watanabe *et al*., 1994; Warner *et al*., 1996; Wong *et al*., 1998).

The dynamical effects of these processes on the ventilation of the North Pacific intermediate layer have been investigated using numerical models. By implicitly taking the effects of the above processes into account, restoration of model temperature and salinity in the Okhotsk Sea to the observed values can drive the Oyashio southward to cross over the wind-driven gyre boundary determined by the Sverdrup flow (Mitsudera *et al*., 2004), resulting in the freshening of NPIW (Yamanaka *et al*., 1998). Comparison of the results of numerical experiments with and without tidally induced vertical mixing at the Kuril Straits suggests that tidal mixing there can strengthen the ventilation in the Okhotsk Sea and the North Pacific (Nakamura *et al*., 2004, 2006a, 2006b, hereafter the latter reference is referred to as NTIA06). The enhanced ventilation in the Okhotsk Sea takes place through downward diffusion and an enhancement of the convection resulting from a preconditioning of salinity values due to an upward salt flux caused by tidal mixing from the saltier lower layer. The preconditioned (i.e., saltier) water leads to an increase in the density of the water involved in convection and thus an increase in the volume of the water reaching the intermediate layer. The ventilated water flows into the North Pacific and spreads over the entire subarctic and most of the subtropical gyres, enhancing ventilation of the intermediate layer.

It is interesting that, in association with the inflow of the ventilated water from the Kuril Straits, the flow pathways in the intermediate layer were also modified to further enhance the ventilation in their model results. The key elements of the dynamics in the change of the flow pathways were identified by NTIA06 and Nakamura *et al*. (2004). The forcing is by diapycnal mass transport from the shallower and deeper layers to the intermediate layer due to tidally enhanced vertical diffusion and convection. The downward diffusion induces a counterbalancing upwelling from the deeper layers, and thus mainly excites the first baroclinic mode response (more precisely, since the vertical profile of density around the Kuril Straits is concave upwards, vertical diffusion generally decreases density and hence produces a net mass flux to the lighter, shallower layers). On the other hand, convection brings surface water into the intermediate layer, and hence excites the second and higher baroclinic mode responses.

The dynamical adjustment to the forcing proceeds mainly through coastally trapped waves such as Kelvin waves and eastward-moving (or advected) long-Rossby waves, which develop as a result of the wind-driven circulation for the second and higher modes. The Kelvin waves induce a flow towards the equator in the intermediate layer along the western boundary that induces inter-gyre transport of the ventilated water from the Kuril Straits to the subtropical gyre (other kinds of coastally trapped waves that are faster than the local currents also have a similar effect). The transported water turns eastward and flows around the interior region, where the eastward long-Rossby waves carry dynamical information of the inflow to modify circulation there. The water eventually leaks into the equatorial region and subsequently to the other oceans. Tatebe and Yasuda (2004) constructed an analytical model, which relates the Oyashio southward intrusion (and associated cross gyre transport) to the diapycnal upwelling.

However, in spite of the need for both Kelvin and Rossby waves in the intermediate layer adjustment in the North Pacific, previous theories have not considered the two simultaneously. Earlier work on ventilation may be categorized into the ventilated thermocline type represented by Luyten *et al*. (1983) and Rhines and Young (1982), which emphasize the effect of wind driven circu-

lation, and abyssal circulation theories along the lines of Stommel and Arons (1960) and Kawase (1987), which focus on the effect of mass input/output due to thermohaline forcing.

The ventilated thermocline theory does include the effect of eastward long-Rossby waves on wind-driven gyres, but the western boundary is absent in most of these theories. Such works do not, therefore, consider the effect of Kelvin waves or the inter-gyre flow through the western boundary region, even though inter-gyre flows taking place in the interior have been extensively investigated (e.g., Pedlosky, 1984; Schopp and Arhan, 1986; Luyten and Stommel, 1986; Schopp, 1988, 1993; Chen and Dewar, 1993). Although some theories include a western boundary (e.g., Young and Rhines, 1982; Hogg and Stommel, 1985; Huang, 1990; Jarvis and Veronis, 1994), the effect of mass input is absent, thus the inter-gyre flow is not considered. Huang and Flierl (1987) show that the semigeostrophic effect allows the subpolar western boundary current to intrude into the subtropical gyre in the presence of outcropping. In the absence of mass input, however, all of the water making up this intrusion should return to the subpolar region, which is not the case for the North Pacific intermediate layer.

Although the abyssal circulation theory does incorporate the effect of mass-driven Kelvin waves as a deep western boundary current, the effect of wind-driven circulation is omitted in most of the theories (e.g., Straub and Rhines, 1990; Pedlosky, 1992; Speer and McCartney, 1992; Straub *et al*., 1993; Pedlosky and Chapman, 1993; Ishizaki, 1994; Edwards and Pedlosky, 1995; Cember, 1998). Some of these works include the effect of eastward propagating long-Rossby waves due to bottom topography and improve our understanding of the basic dynamics. Hautala and Riser (1989) consider the effect of wind, but their attention is limited to the shadow region, and hence the effect of eastward long-Rossby waves is neglected.

In this paper we develop, in a rather heuristic manner, a simple analytical model to investigate the effects of mass input/output from the western boundary on the intermediate layer, by incorporating the effects of both Kelvin and eastward long-Rossby waves using a 2.5 layer model with a western boundary. The focus of the study is the area of the North Pacific. Our simple model is a first step toward unifying the two branches of the ventilation theory and toward a better understanding of the mechanism by which the stratification is maintained in the intermediate density layer between the outcropping component in the subtropics and the portion ventilated by deep convection. (The former is described in the ventilated thermocline theory, and the latter in the abyssal circulation theory.)

The paper is organized as follows. The design of the 2.5 layer model is described in Section 2. Solution of the "barotropic" mode and its properties are presented in Section 3. Characteristic curves (geostrophic contours) and a solution for the upper and lower layers (and their properties) are shown in Section 4. The results are summarized and discussed in Section 5. The implications of various parameter regimes are presented in Appendices.

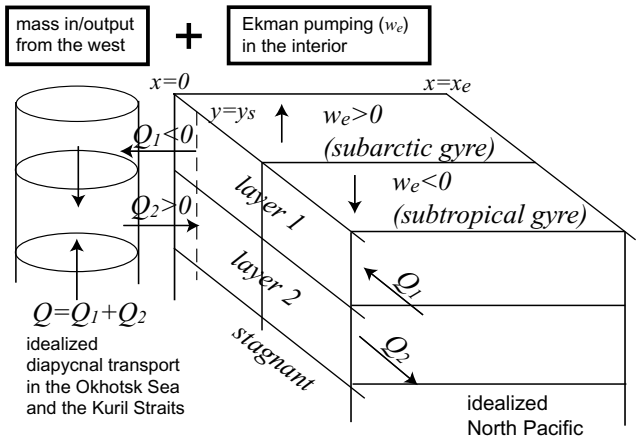

Fig. 2. Schematic of the 2.5 layer model.

2. Model Design

2.1 2.5-layer QG model

In order to illustrate the essential physics as simply as possible, we consider a steady quasigeostrophic (QG) model on a β plane.

In the vertical direction, a 2.5 layer model is chosen. Crudely speaking, this approach resolves the first and second baroclinic modes, and is the simplest model capable of describing the eastward-moving long-Rossby waves due to wind driven circulation, which play a crucial role in the adjustment of the interior region, as revealed in NTIA06. Although forcing also comes from the higher modes in the numerical model results of NTIA06, the higher modes may be considered to represent a quantitative correction to the second mode. This is because the dynamical role of the higher modes is similar to that of mode 2, in the sense that all of these modes allow eastward moving long-Rossby waves in the region of a strong eastward Sverdrup flow.

A schematic of the 2.5 layer model considered here is shown in Fig. 2. The model domain includes both subpolar and subtropical gyres and is open on the equatorial side. The domain is bounded on the east and west at $x = x_e$ and $x = 0$, respectively, through which no geostrophic flow is allowed. The upper moving layer (hereafter the upper layer or layer 1) is supposed to surmount the lower moving layer (hereafter the lower layer

or layer 2) everywhere, so that the lower layer does not outcrop to the sea surface in the model domain, as is actually the case for the NPIW.

2.2 Forcings

We consider two kinds of external forcing. One is Ekman pumping, w_e, imposed at the sea surface. The other forcing is a mass source associated with the convergence/divergence of diapycnal transport produced by both the convection in the Okhotsk Sea and vertical mixing at the Kuril Straits. The convection causes diapycnal transport from the lighter, surface layer to the heavier, intermediate layer. Vertical mixing at the Kuril Straits can cause both enhancement of the convection and upwelling from the deeper layers, which balances downward diffusion. The former works in a similar fashion to the convection itself, while the latter produces a net mass flux into the intermediate layer from the deeper layers. Associated vertical mass convergence in the intermediate layer (or divergence in other layers) induces a mass flux to (or from) the North Pacific in the corresponding layer. This is idealized as a mass source that feeds fluid of the corresponding density into layer n at a rate Q_n from the western boundary at latitude y_s (it works as a sink when Q_n is negative).

Note that because the effect of third-layer motion on the other layers is neglected in a 2.5 layer model, motion of the mass sink from the third layer is also neglected. Nevertheless, this ineffective mass sink balances the water budget between the North Pacific and the Okhotsk Sea. Also, any across-interface velocity component is neglected in the domain under consideration. Diapycnal transport, which includes the cause of the above mass source/sink and is required to maintain the basic stratification, is supposed to take place out of the domain.

Since the numerical model results of NTIA06 suggest that the Kelvin waves and the associated change in the flow along the western boundary can remove the mass fed from the source, we include a western boundary region. This is done by adding a frictional western boundary layer, following Liu *et al*. (1999). The frictional layer used here is the Munk layer (Munk, 1950), since this is a simplest possible theory of the western boundary current that can represent the effect of both the Kelvin and damping short-Rossby waves. Friction is neglected in the interior.

The mass flux originating from the above source (or sink) is supposed to leave (or enter) the model domain through the equatorward boundary, so that the volume of each layer is held constant (i.e., the mass is conserved). This assumption is based on the results of the experiments in NTIA06, which suggest that most of the southward Kelvin waves and associated mass flux leave the North Pacific for the Indian Ocean and the South Pacific. The Kelvin waves that leave the North Pacific decay as they circulate in other basins. Consistent with this picture, the NPIW is actually observed to leak into the Indonesian Through Flow where it is transformed (Lukas *et al*., 1991; Ffield and Gordon, 1992). Thus, the water that left the domain is supposed to be transformed in other basins and to return through other layers. Although a small fraction of the Kelvin-wave energy can propagate northward along the east coast of the North Pacific, as seen in the numerical model result (NTIA06), the effect of this is assumed to be included through the layer thickness at the eastern boundary.

2.3 Equations

The vorticity equations, which govern the system, are

$$J(\psi_1, q_1) = \frac{f_0}{H_1} w_e + \mathbf{k} \cdot \nabla \times \mathcal{F}_1, \tag{1}$$

$$J(\psi_2, q_2) = \mathbf{k} \cdot \nabla \times \mathcal{F}_2, \tag{2}$$

where the subscripts 1 and 2 indicate the upper and lower layers, respectively (e.g., Pedlosky, 1987, 1996). Here, ψ is the streamfunction, and q is the potential vorticity (PV). Since our focus is on gyre-scale motion, the effect of relative vorticity is negligible in comparison with that of planetary vorticity, so that q can be approximated as

$$q_1 = \beta y + F_1(\psi_2 - \psi_1), \tag{3}$$

$$q_2 = \beta y + F_2(\psi_1 - \psi_2) - G_2\psi_2, \tag{4}$$

where,

$$F_n = \frac{f_0^2}{\gamma_1 H_n}, \tag{5}$$

$$G_n = \frac{f_0^2}{\gamma_2 H_n}, \tag{6}$$

$$\gamma_n = \frac{\rho_{n+1} - \rho_n}{\rho_0} g, \tag{7}$$

$f_0 + \beta y$ is the Coriolis parameter on the β plane, H_n is the mean thickness of layer n, ρ_0 is the reference density, and g is the gravity acceleration. The vector $\mathbf{k}$ represents the unit in the vertical direction, and $\mathcal{F}_n$ is a horizontal frictional force in layer n which is given in the western boundary region.

3. "Barotropic" Mode (or Mode 1)

3.1 Solution of "barotropic" mode

Firstly, the "barotropic" mode roughly corresponding to mode 1 is examined. In the interior, the vertical average of the vorticity equations yields the Sverdrup balance:

$$\beta \frac{\partial \psi_b}{\partial x} = \frac{f_0}{H} w_e, \tag{8}$$

where H is the total thickness of the moving layers ($H = H_1 + H_2$) and

$$\psi_b = \frac{H_1 \psi_1 + H_2 \psi_2}{H} \tag{9}$$

is the barotropic streamfunction. Near the western boundary, a boundary-layer correction in the form of a Munk layer is added:

$$\beta \frac{\partial \psi_b}{\partial x} = A_h \frac{\partial^4 \psi_b}{\partial x^4}, \tag{10}$$

where A_h is a horizontal eddy viscosity coefficient. The Ekman pumping term is neglected, assuming that it is small in comparison with the friction term.

Since these equations are linear, ψ_b can be separated into a wind driven component ($\psi_b{}^w$) and a component driven by the mass source ($\psi_b{}^m$):

$$\psi_b = \psi_b^w + \psi_b^m. \tag{11}$$

The wind driven component is the same as that obtained in the absence of the mass source. It is hence given as

$$\psi_b^w = \psi_b^i(x,y) - \psi_b^i(x,y)\phi_m(x), \tag{12}$$

where $\psi_b{}^i$ is the streamfunction of the Sverdrup flow in the interior,

$$\psi_b^i = -\frac{f_0}{\beta H}\int_x^{x_e} w_e(x',y)dx', \tag{13}$$

and ϕ_m represents the zonal structure of the Munk layer,

$$\phi_m = \exp\left(-\frac{x}{2\delta_m}\right)\left[\cos\left(\frac{\sqrt{3}x}{2\delta_m}\right) + \frac{1}{\sqrt{3}}\sin\left(\frac{\sqrt{3}x}{2\delta_m}\right)\right]. \tag{14}$$

Here, δ_m is the thickness scale of the Munk layer ($\delta_m = (A_h/\beta)^{1/3}$), and a no-slip condition is imposed at the western boundary.

The mass-driven component of the barotropic mode is contained in the western boundary layer, where the mass source is located and friction is present. In fact, the mass-driven barotropic flow is zero in the interior, similar to the model of Kawase (1987). This is because it is governed by $\beta\partial\psi_b{}^m/\partial x = 0$ in the interior, which results in $\psi_b{}^m$ of an arbitrary constant when combined with the no-normal flow condition at the eastern boundary ($\partial\psi_b{}^m/\partial y = 0$). Accordingly, $\psi_b{}^m$ can be set to be zero in the interior.

The mass-driven component carries the mass flux from the source, and thus the zonally integrated meridional volume transport of this component is Q, where $Q = Q_1 + Q_2$. Such a mass flux takes place equatorward of the mass source through the Kelvin wave dynamics (since the effect of Kelvin waves propagating around the basin is not explicitly considered). Since the mass flux leaves the domain through the equatorward boundary, the mass conservation constraint is assured by the combination of the conditions for zonally integrated volume transport due to $\psi_b{}^w$ and $\psi_b{}^m$.

Under the above two conditions—(i) $\psi_b{}^m$ approaches to zero away from the western boundary and (ii) the zonally integrated meridional volume transport is Q equatorward of y_s—together with no-normal flow and no-slip conditions at the western boundary, $\psi_b{}^m$ is obtained from (10) in a similar way to the Munk solution as

$$\psi_b^m = \frac{Q}{H}\phi_{ys}(y)\phi_m(x). \tag{15}$$

Here, the meridional structure function $\phi_{ys}(y)$ is defined as

$$\begin{aligned} \phi_{ys}(y) &= 1, \quad \text{for } y \le y_s, \\ &= 0, \quad \text{for } y > y_s, \end{aligned} \tag{16}$$

and the zonal structure is that of the Munk layer. Taking these two structures together, (15) reflects the fact that Kelvin wave activity redistributes the input mass along the western boundary on the equator side of the mass source, leading to the formation of a mass-driven western boundary current. The amplitude of the latter is determined from the net mass influx divided by the total mean layer thickness.

Combining the two components, we obtain the streamfunction of the barotropic mode,

$$\psi_b = \psi_b^i(x,y) - \left[\psi_b^i(x,y) - \frac{Q}{H}\phi_{ys}(y)\right]\phi_m(x). \tag{17}$$

3.2 *Properties of the "barotropic" mode solution*

Prior to considering the "baroclinic" mode solution, the properties of the barotropic mode solution are examined, since these determine the characteristic curves of ψ_2 in the QG dynamical framework under consideration.

The solution (17) consists of the Sverdrup interior, its western boundary layer correction, and the mass driven component. Since the last two components are confined near the western boundary, the interior flow is not affected by the mass input for the barotropic mode. We thus examine the western boundary currents in the presence of the mass source, before presenting an overall pattern of the barotropic mode flow. It should be noted that this unchanged interior flow is different from the results usually obtained by abyssal circulation theories. The difference arises from the present model settings, in which both temporal change in layer thickness and mass transport across the layer interface are absent.

3.2.1 *Confluence point of the western boundary currents*

A schematic of how the western boundary current is composed of the wind- and mass-driven components is presented in Fig. 3(a). The wind-driven component $(-\psi_b^i(x, y)\phi_m)$ compensates the convergence (or divergence) of the Sverdrup transport through its variation in transport. Although the mass driven component, $(Q/H)\phi_m$, merely adds a constant transport, its contribution is important since it enables a western boundary current to cross the boundary of the subpolar and subtropical gyres. The latter is defined by the isoline $\psi_b^i = 0$ (e.g., Schopp and Arhan, 1986) and becomes a zonal line $y = y_{gb}$ near the western boundary in the present case. When $Q = 0$, the gyre boundary is collocated with the edge of the boundary of the western boundary currents. In contrast, when $Q \neq 0$, the solution (17) indicates that the meridional velocity of the Munk layer is no longer zero at y_{gb} as it now disappears at meridional positions where

$$H\psi_b^i(x, y) = Q. \tag{18}$$

Accordingly, the confluence point of the western boundary currents of the subpolar and subtropical gyres, if it exists, moves to the meridional position, y_{cwbc}, which satisfies (18) and is closest to y_{gb} for the same x, or moves to y_s when $Q << 0$. From the dynamical point of view, the confluence moves to the latitude where the given net-mass flux is compensated by the Sverdrup flow. This result is essentially equivalent to that obtained by Tatebe and Yasuda (2004).

To consider the spatial shift of y_{cwbc} in more detail, the relationship between the mass influx Q, the Sverdrup transport at the western boundary T_{Sv}, and y_{cwbc} is shown schematically in Fig. 3(b). When $Q \geq 0$, the position of y_{cwbc} can be categorized into three cases:

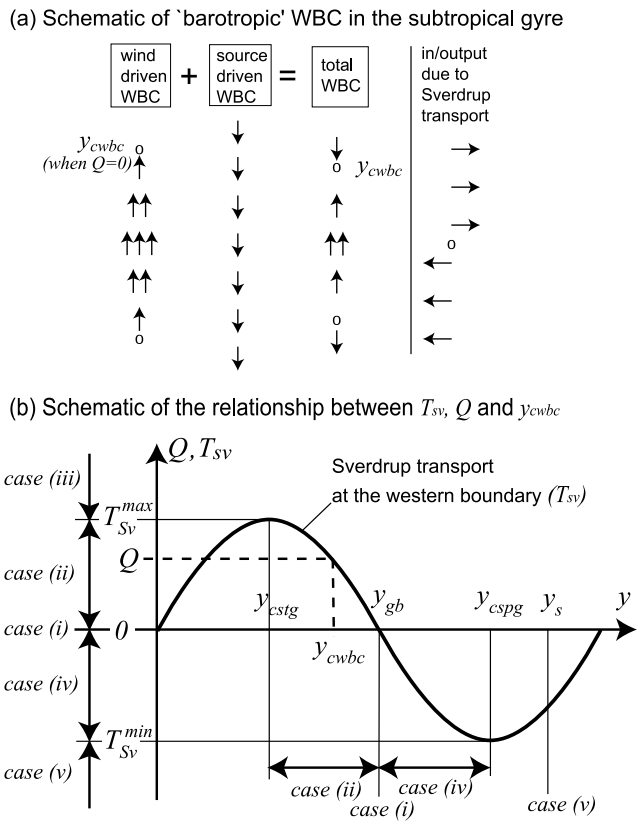

Fig. 3. (a) Schematic of the "barotropic" mode western boundary current driven (left to right) by a mass source, by wind, and in total for a moderate mass input (i.e., case (ii)). (b) Schematic of the relation between Sverdrup transport at the western boundary (T_{Sv}), the net mass influx (Q), and the latitudinal position of the confluence of the subpolar and subtropical western boundary currents (y_{cwbc}). A schematic distribution of T_{Sv} is shown as a function of y. y_{cwbc} is determined from Q and T_{Sv}, as indicated as an example by dashed lines. y_{cwbc} can thus be categorized according to Q and T_{Sv} into five cases as shown in the left. In each case, y_{cwbc} is located as shown at the bottom.

(i) $y_{cwbc} = y_{gb}$, when $Q = 0$: The confluence y_{cwbc} is at the gyre boundary, when the net mass input is zero.

(ii) $y_{cstg} < y_{cwbc} < y_{gb}$, when $0 < Q < T_{Sv}^{max}$: The confluence y_{cwbc} is in the northern part of the subtropical gyre for a moderate mass input. The quantity T_{Sv}^{max} denotes the maximum Sverdrup transport in the subtropical gyre, whereas y_{cstg}, its latitude, represents the center of both the subtropical gyre and the pool region there if it exists. This case corresponds to that of the North Pacific.

(iii) y_{cwbc} is absent in the domain, when $Q \geq T_{Sv}^{max}$: When the net mass influx is larger than the maximum Sverdrup transport, the western boundary current flows equatorward throughout the subtropical gyre, and reaches the equatorial region. In other words, a confluence of the

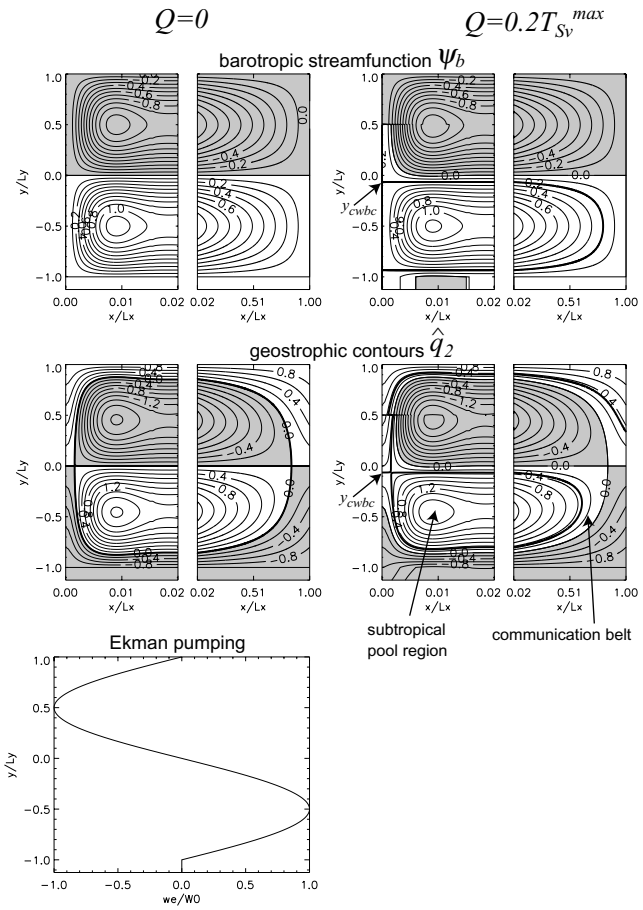

Fig. 4. (Top) "Barotropic" mode streamfunction, ψ_b, and (middle) geostrophic contours, $\hat{q}_2$. (Left) The case (i) when $Q = 0$ and (right) the case (ii) when $0 < Q < T_{Sv}^{max}$. T_{Sv}^{max} is the maximum Sverdrup transport. ψ_b, $\hat{q}_2$, x, and y are nondimensionalized by T_{Sv}^{max}/H, βL_y, L_x, and L_y, respectively. Shaded areas denote negative values. The Ekman pumping used is shown at the bottom of the figure. The thick lines in the case with mass input represent the isolines of $\psi_b = Q/H$ and $\hat{q}_2 = \beta y_{cwbc} + \hat{F}\,Q/H$. Details are written in the text.

subpolar and subtropical western boundary currents does not exist. Such strong diapycnal transport rarely occurs in major basins.

When $Q < 0$, the net mass flux works as a sink, and hence the position of y_{cwbc} moves poleward toward the mass sink. In this case the position also depends on the location of the sink, because the mass-driven flow is induced only on the equator side of y_s through the Kelvin wave dynamics. Accordingly, the northern limit of the position of y_{cwbc} is fixed at y_s regardless of the magnitude of the mass output. (The confluence could move further north if we allowed a portion of the Kelvin wave to circulate around the domain.) Associated with this, the threshold value of Q, which dictates whether y_{cwbc} is at y_s or further to the equator, becomes T_{Sv}^{min} when $y_s > y_{cspg}$ or T_{Sv}^{ys} when $y_s < y_{cspg}$. Here, T_{Sv}^{min} is the minimum Sverdrup transport taking place at y_{cspg}, the center of the subpolar gyre, and T_{Sv}^{ys} is the Sverdrup transport at y_s. Thus, writing the condition for the latter case in parentheses, the position of y_{cwbc} can be categorized into the following two additional cases:

(iv) $y_{gb} < y_{cwbc} < y_{cspg}$ (or y_s), when T_{Sv}^{min} (or T_{Sv}^{ys}) $< Q < 0$: The confluence y_{cwbc} is in the southern part of the subpolar gyre, when the mass source works, on the whole, as a moderate sink. This situation could be realized by the occurrence of strong deep convection, which brings the upper layer water to the deep layer.

(v) $y_{cwbc} = y_s$, when $Q \le T_{Sv}^{min}$ (or T_{Sv}^{ys}): The confluence y_{cwbc} is located at y_s for such a large mass output.

In the following, we focus on case (ii) together with case (i) for comparison. A discussion of the other cases is given in Appendix 1.

3.2.2 Flow pattern of the "barotropic" mode

In order to show a typical flow pattern of the barotropic mode, we consider here a simple case in which w_e is a function only of y with a form,

$$\begin{aligned} w_e &= -W_0 \sin\frac{\pi}{L_y} y, \quad \text{for } -L_y \le y \le L_y, \\ &= 0, \qquad\qquad \text{for } y < -L_y,\ L_y < y. \end{aligned} \tag{19}$$

The gyre boundary is set on $y = y_{gb} = 0$, and the subpolar and subtropical gyres range from $0 < y < L_y$ and $-L_y < y < 0$, respectively.

Further, ψ_b is nondimensionalized by T_{Sv}^{max}/H as,

$$\tilde{\psi}_b = \tilde{\psi}_b^i(\tilde{x},\tilde{y}) - \left[\tilde{\psi}_b^i(\tilde{x},\tilde{y}) - \frac{Q}{T_{Sv}^{max}}\phi_{ys}(\tilde{y})\right]\phi_m(\tilde{x}), \tag{17′}$$

where

$$\frac{T_{Sv}^{max}}{H} = \frac{f_0 L_x W_0}{\beta H}. \tag{20}$$

Here, $\tilde{()}$ indicates a nondimensional variable, x and y are nondimensionalized by L_x and L_y, respectively, and x_e is set to L_x. According to (17′), the barotropic mode solution is controlled by only two nondimensional parameters, Q/T_{Sv}^{max} and δ_m/L_x, once y_s is specified. The former is introduced in this study and measures the relative contribution to the western boundary current due to mass input and wind forcing. The latter is the ratio of the Munk layer thickness and the basin width.

Figure 4 shows the distribution of ψ_b for cases (i)

Table 1. Parameters.

Notations	Parameters	Values
	Nondimensional parameters	
δ_m/L_x	nondimensional Munk layer width	0.0025
Q/T_{Sv}^{max}	inter-gyre boundary and communication	0.2
α	extent of pool regions	2
Q_2/Q	vertical structure of mass-driven flow	1.5
H_2/H	background stratification	0.6
$\hat{F}/G_2$	background stratification	0.3
	Dimensional parameters	
δ_m	Munk layer width	20 km
A_h	horizontal viscosity coefficient	2×10^2 m^{2}s^{-1}
L_x	zonal extent of the basin	8,000 km
L_y	meridional extent of a gyre	2,000 km
T_{Sv}^{max}	maximum Sverdrup transport in the subtropical gyre	30–50 Sv
Q	net mass flux into layers 1 and 2	1–8 (or ~3) Sv
Q_2	mass flux into the lower layer	~6 Sv
$\hat{F}$	defined in (24)	3×10^{-9} m^{-2}
β	gradient of Coriolis parameter	2×10^{-11} m^{-1}s^{-1}
H	total thickness of layers 1 and 2	1,000 m
H_2	thickness of the lower layer	600 m
γ_1	reduced gravity	0.015 m s^{-1}
G_2	defined in (6)	1×10^{-8} m^{-2}

Values of nondimensional parameters used in case (ii) and rough estimates of dimensional parameters for the North Pacific intermediate layer.

and (ii). The values of Q/T_{Sv}^{max} and δ_m/L_x are set to be 0.2 and 2.5×10^{-3}, respectively, and are shown in Table 1 with values of dimensional parameters. Although the value of Q/T_{Sv}^{max} would be larger than a realistic value*, it is chosen for the clarity of the figure and because the solution does not change qualitatively for $0 < Q/T_{Sv}^{max} < 1$, as is argued in the previous section.

Although the streamfunction in the interior remains the same, the mass-driven flow affects the starts and ends of the streamlines. Those paths emanating from the mass source intrude from the subpolar region into the subtropics along the western boundary, enter the interior to circulate through the outer rim of the subtropical gyre, and finally leave the subtropics to move to the equatorial region along the western boundary. Note that the above path is different from that of the Kelvin waves which cause dynamical adjustment to the mass input, as expected from Fig. 3.

4. Lower Layer Circulation

4.1 Equations of ψ_2

Given ψ_b in the previous section, ψ_1 can be rewritten as,

$$\psi_1 = \frac{H\psi_b - H_2\psi_2}{H_1}. \tag{21}$$

This enables the lower layer equations to be written in terms of ψ_2, whose solution in turn yields ψ_1.

4.1.1 In the interior

In the interior, approximated here as an inviscid region, the governing equation becomes

*The annual mean Sverdrup transport in the subtropical gyre of the North Pacific is in the range of 30–50 Sv (1 Sv = 10^6 m^3 s^{-1}; e.g., Aoki and Kutsuwada, 2008). Changes in the strength of the meridional overturning due to tidal mixing at the Kuril Straits, which may give an estimate of Q, are 1–8 Sv and ~3 Sv for all experiments and the main experiment in NTIA06, resulting in Q/T_{Sv}^{max} of around 0.02–0.27 or 0.06–0.1, respectively.

$$J(\psi_2, \hat{q}_2) = 0, \tag{22}$$

where

$$\hat{q}_2 = \beta y + \hat{F}\psi_b, \tag{23}$$

$$\hat{F} = \frac{f_0^2 H}{\gamma_1 H_1 H_2}, \tag{24}$$

$$q_2 = \hat{q}_2 - \left(\hat{F} + G_2\right)\psi_2. \tag{25}$$

As reviewed by Pedlosky (1996), isolines of $\hat{q}_2$ are characteristic curves of (22) and are often called geostrophic contours, along which both the geostrophic streamfunction and PV in layer 2 (i.e., ψ_2 and q_2) are conserved in the nondissipative limit. Since this dynamical aspect of the geostrophic contours is usually understood in terms of long-Rossby waves, we call this inviscid component a "long-Rossby wave" in the following and write the streamfunction and PV associated with this component as ψ_2^{lr} and q_2^{lr}, respectively.

In order to allow the lower layer in the interior to be in motion, there must be a so-called pool region, which is shielded from the geostrophic contours emanating from the eastern boundary (e.g., Rhines and Young, 1982). Otherwise, the shadow zone, where the geostrophic contours transmit the eastern boundary condition, covers the whole interior, and hence motion in the lower layer, if any, is confined near the western boundary regardless of the presence of mass source under the present QG approximation. Our interest is thus in the case with a pool region. The condition of the presence of a pool region is that a point exists which satisfies

$$-\frac{\partial \psi_b}{\partial y} > \frac{\beta}{\hat{F}} \tag{26}$$

somewhere in the gyres, thus an eastward Sverdrup flow can arrest westward propagating Rossby waves (e.g., Pedlosky, 1996). The following discussion concentrates on the case in which this condition is met.

4.1.2 Near the western boundary

Firstly, let us consider a situation without mass input. Even in this case, the absence of adequate theories of the western boundary current makes it very difficult to give a completely convincing argument for closing the circulation through the western boundary region. Nevertheless, in order to gain an insight which could be helpful for future development of more rigorous arguments, we make a simplifying assumption that friction can be neglected in the lower layer even in the western boundary region. This is associated with the assumption that friction in the upper layer is given by $A_h(\partial^4\psi_1/\partial x^4) + A_h\,(H_2/H_1)(\partial^4\psi_2/\partial x^4)$.

In other words, we consider the case in which friction in the lower layer is so small that the characteristic curves are not greatly altered although the information passing through the characteristics would be slightly modified. This condition may be met when $\mathbf{c}\cdot\nabla q_2 >> A_2\nabla^4\psi_2$ where $\mathbf{c}$ is the phase velocity of long Rossby waves of the second or higher modes and A_2 is the horizontal eddy viscosity coefficient in layer 2. Scaling the width of the western boundary region l as ~50 km, the deformation radius L_d as ~50 km, the meridional scale L_y as 2000 km, and the meridional component of $\mathbf{c}$, c_y as 2 cm s^{-1}, A_2 should satisfy $A_2 << c_y(l^4/L_yL_d^2) \sim 2500$ m^{2}s^{-1}, which may not be a very unrealistic value. A similar value may be obtained from a comparison of the viscous and β terms. Note that a coarse resolution model of NTIA06, whose results motivated this study, set A_h as 1000 m^{2}s^{-1} and narrowly satisfied this condition, and more recent models having higher resolutions usually meet the condition.

If we assume that friction is negligible, the lower layer circulation can be closed, since there is no PV input in the lower layer if thermohaline forcing is absent. In fact, since ψ_b takes the same value at the eastern and western boundaries (due to the constraint that no net meridional volume transport is induced by the wind), (23) indicates that the isolines of $\hat{q}_2$ in a pool region must be closed before reaching the western boundary, and hence those of ψ_2^{lr} are closed. The western boundary is outside the pool region but in the shadow zone, and the fluid is stagnant there. Hence, a frictional western-boundary current is not required in the lower layer in this case.

When $Q_2 \neq 0$ (i.e., the mass source is present in the lower layer), a western boundary current is required to carry the additional mass flux along the western boundary, as seen in the numerical model result (NTIA06). Thus, we also introduce the Munk layer in the lower layer as in the barotropic mode and assume that the lower layer circulation consists of the long-Rossby wave component and the Munk layer component (ψ_2^{wbc}), with the latter including the component influenced by friction or representing the flow induced by the Kelvin-wave adjustment. That is,

$$\psi_2 = \psi_2^{lr} + \psi_2^{wbc}, \tag{27}$$

where ψ_2^{lr} and ψ_2^{wbc} are governed, respectively, by

$$J\left(\psi_2^{lr}, \hat{q}_2\right) = 0, \tag{28}$$

and

$$\beta \frac{\partial \psi_2^{wbc}}{\partial x} = A_h \frac{\partial^4 \psi_2^{wbc}}{\partial x^4}. \quad (29)$$

Note that, similarly to the effect of viscosity, the presence of ψ_2^{wbc} may also distort the characteristics of ψ_2^{lr}. When the current velocity associated with ψ_2^{wbc} is weak, the characteristics are not significantly affected. We shall consider this case further below. On the other hand, when the velocity component associated with ψ_2^{wbc} is stronger than that associated with ψ_2^{lr}, ψ_2^{lr} obtained from (28) is no longer valid in the western boundary region. Instead, the current is dominated by the ψ_2^{wbc} component in this case, and thus the dominant feature would be captured.

4.2 Geostrophic contours

The distribution of geostrophic contours is examined to obtain an insight into the response of the lower layer to the mass source.

4.2.1 Parameter settings

Examples of the distribution of $\hat{q}_2$ for cases (i) and (ii) are shown in Fig. 4. The settings are common to those of ψ_b (the other cases are shown in Appendix 1).

For these figures, a third nondimensional parameter related to a pool region (α) appears through the nondimensionalization of (23) by βL_y as,

$$\tilde{\hat{q}}_2 = \tilde{y} + \alpha \tilde{\psi}_b, \quad (30)$$

where

$$\alpha = \frac{\hat{F}}{\beta L_y} \frac{T_{Sv}^{max}}{H} = \frac{f_0^3 L_x W_0}{\beta^2 L_y \gamma_1 H_1 H_2}. \quad (31)$$

This parameter measures the relative contribution to potential vorticity of the thickness variation due to the wind forcing and the planetary vorticity gradient, and thus determines the area of a pool region (e.g., Pedlosky, 1996). This is set to 2, which is relevant to the situation of the NPIW.

4.2.2 Properties of $\hat{q}_2$

To illustrate the effect of mass input, the wind-only case is shown first. When $Q = 0$, the pool regions in the subpolar and subtropical gyres are symmetric due to the QG approximation. The geostrophic contours emanating from the eastern boundary meet the western boundary at the same latitude and make the boundary the shadow zone, as argued in the previous section.

In contrast, when $Q \neq 0$, geostrophic contours are deflected further due to the mass-driven barotropic flow. Firstly, due to the "barotropic" mass influx, geostrophic contours near the western boundary turn to the interior at $y = y_s$, and then towards the south. Although the deflected contours in the nearshore region soon hit the western boundary, some of those in the offshore region cross the gyre boundary at $y = y_{gb} = 0$, and subsequently penetrate into and circulate around the outer rim of the region (corresponding to the subtropical pool region when $Q = 0$) and finally encounter the western boundary, thereby forming a belt-like shape. These contours therefore connect the subpolar to subtropical gyres in a region we define as the "communication belt". Associated with this, the subtropical pool region, in which geostrophic contours are closed, undergoes a contraction, while the subpolar pool remains almost the same.

More precisely, the communication belt represents the zone covered by the family of geostrophic contours that pass through the line $y = y_s$ between the western boundary and the subpolar pool region and includes the nearshore part, where geostrophic contours do not reach the interior. This definition of the communication belt is rather convenient for obtaining a solution. Also, the lower layer current in the nearshore part is able to flow into the subtropics when the component ψ_2^{wbc} is added, as shown in Subsection 4.4.2.

The communication belt is thus adjacent to the subpolar pool region and to the subtropical shadow zone. The boundary on this side is given by the isolines,

$$\hat{q}_2 = \beta y_{gb}, \quad (32)$$

as in the $Q = 0$ case, since ψ_b and hence the geostrophic contours in the interior remain the same in the present QG dynamics. On the other side, the communication belt is bounded by the subtropical pool region and by the western boundary. The former boundary is given by the geostrophic contours connected to the point ($x = 0$, $y = y_{cwbc}$) where $\psi_b = Q/H$, that is,

$$\hat{q}_2 = \beta y_{cwbc} + \hat{F} \frac{Q}{H}, \quad (33)$$

for the following reason. On the line $y = y_{cwbc}$, the barotropic western boundary current has no meridional component (because of the neglect of Ekman pumping in the western boundary region), and thus the geostrophic contour extending along $y = y_{cwbc}$ from the western boundary reaches the interior. This contour then connects with the geostrophic contour in the northern part of the region that would define the subtropical pool region in the case $Q = 0$, since we are considering case (ii) in which y_{cwbc} is located between y_{gb} and y_{cstg} (Fig. 3). The contour thus encircles the subtropical pool region and forms its boundary with the communication belt, as shown in Fig. 4 using the thick line.

Note also that as the barotropic flow leaks out to the

equatorial region due to the mass-driven component, the shadow zone also extends into the equatorial region near the western boundary. Thus, the effects of the eastern boundary condition are communicated to the equatorial region.

4.3 Determination of ψ_2

Similar to the case of ψ_b, ψ_2 can be obtained as

$$\begin{aligned}\psi_2 &= \psi_2^{lr} + \psi_2^{wbc} \\ &= \psi_2^{lr} + \left[\frac{Q_2}{H_2} - \psi_2^{lr}(x=0)\right]\phi_{ys}(y)\phi_m(x),\end{aligned} \tag{34}$$

where $\psi_2{}^{lr}$ ($x = 0$) is the value at the western boundary and we use the condition that the zonally-integrated meridional transport in layer 2 is Q_2 equatorward of y_s. Note that the above condition ensures the mass conservation relation in layer 2 (and thus in layer 1 when combined with the corresponding condition for the barotropic mode).

The component $\psi_2{}^{lr}$ is written from (25) as

$$\psi_2^{lr} = \frac{\hat{q}_2 - q_2^{lr}}{\hat{F} + G_2}, \tag{35}$$

where $q_2{}^{lr}$ is the PV associated with $\psi_2{}^{lr}$, and we used the assumptions that both $\psi_2{}^{lr}$ and $q_2{}^{lr}$ are constant along the geostrophic contours except at the entry of the mass inflow, and that these are identical to ψ_2 and q_2 in the interior, respectively. The component $\psi_2{}^{lr}$ is then determined using the approximation of PV homogeneity in the pool regions and an inflow condition at $y = y_s$.

It should be noted that, theoretically, the PV homogeneity requires both closed characteristics and a uniform PV distribution on the outermost closed characteristics (e.g., Pedlosky, 1996). These conditions may be disturbed in the western boundary region by either friction or the $\psi_2{}^{wbc}$ component. Nevertheless, if a PV flux into the pool region taking place in the interior region is significantly greater than that in the western boundary region, PV values in a large part of the pool region will be close to the value on the pool boundary on the interior side. In this sense, PV homogeneity would be useful as a rough approximation, at least outside the western boundary region. We assume that this condition is met in the following argument in order to obtain an idealized picture of the lower layer circulation as a first step.

The component $\psi_2{}^{lr}$ can be determined, with an inflow condition of the form

$$\psi_2^{lr} = C\frac{\hat{q}_2}{\hat{F} + G_2}, \tag{36}$$

on the line segment $y = y_s$, $0 \le x \le x$ ($\hat{q}_2 = 0$), where C is an arbitrary constant, and x ($\hat{q}_2 = 0$) is the most westerly longitudinal position at which $\hat{q}_2$ is zero. Here, we set

$$C = \frac{Q_2}{H_2}\frac{\hat{F} + G_2}{\beta y_s + \hat{F}\dfrac{Q}{H}} \tag{37}$$

so that the mass input firstly forces the component of $\psi_2{}^{lr}$ at $y = y_s$, that is $\psi_2 = \psi_2{}^{lr}$ at $x = 0$, $y = y_s$.

The above condition yields $\psi_2{}^{lr}$ in the communication belt as

$$\psi_2^{lr} = \frac{Q_2}{H_2}\frac{\hat{q}_2}{\beta y_s + \hat{F}\dfrac{Q}{H}}, \tag{38}$$

because the functional relationship between $\hat{q}_2$ and $\psi_2{}^{lr}$ holds in the communication belt, and $q_2{}^{lr}$ becomes

$$q_2^{lr} = \hat{q}_2\left[1 - \frac{Q_2}{H_2}\frac{\hat{F} + G_2}{\beta y_s + \hat{F}\dfrac{Q}{H}}\right]. \tag{39}$$

From the approximation of PV homogeneity, $q_2{}^{lr}$ in a pool region is equal to its boundary value. For the subtropical pool region, $q_2{}^{lr}$ on the boundary is equal to $q_2{}^{lr}$ at $x = 0$, $y = y_{cwbc}$ given as

$$q_2^{lr} = \left(\beta y_{cwbc} + \hat{F}\frac{Q}{H}\right)\left[1 - \frac{Q_2}{H_2}\frac{\hat{F} + G_2}{\beta y_s + \hat{F}\dfrac{Q}{H}}\right], \tag{40}$$

from (33). Thus, $\psi_2{}^{lr}$ in the subtropical pool region becomes, from (35),

$$\psi_2^{lr} = \frac{\beta(y - y_{cwbc}) + \hat{F}\left(\psi_b - \dfrac{Q}{H}\right)}{\hat{F} + G_2} + \frac{Q_2}{H_2}\frac{\beta y_{cwbc} + \hat{F}\dfrac{Q}{H}}{\beta y_s + \hat{F}\dfrac{Q}{H}}. \tag{41}$$

Similarly, $\psi_2{}^{lr}$ in the subpolar pool region is given as

$$\psi_2^{lr} = \frac{\beta y + \hat{F}\psi_b}{\hat{F} + G_2}, \tag{42}$$

because q_2^{lr} on the boundary is zero.

Beyond these three regions (i.e., the communication belt and the two pool regions), lies the shadow zone, and thus,

$$\psi_2^{lr} = 0, \tag{43}$$

which is the value at the eastern boundary.

For comparison, ψ_2 in the pool regions when $Q = 0$ is readily obtained from the PV homogeneity approximation, namely,

$$\psi_2 = \psi_2^{lr} = \frac{\hat{q}_2}{\hat{F} + G_2} = \frac{\beta y + \hat{F}\psi_b}{\hat{F} + G_2}. \tag{44}$$

This is derived from the facts that $\hat{q}_2 = q_2 = 0$ on the boundaries of the both pool regions, and that ψ_2^{wbc} is zero from the condition of a zonally-integrated meridional transport. In other regions, $\psi_2 = 0$.

4.4 Properties of ψ_2 and ψ_1

4.4.1 Nondimensional form

Before giving examples of ψ_2^{lr}, we nondimensionalize ψ_2^{lr} and ψ_2^{wbc} by T_{Sv}^{max}/H_2, to highlight the influence of external parameters in controlling lower layer transport. This yields

$$\tilde{\psi}_2^{lr} = \left(\frac{Q_2}{Q}\right)\left(\frac{Q}{T_{Sv}^{max}}\right)\frac{\alpha^{-1}\tilde{y} + \tilde{\psi}_b}{\alpha^{-1}\tilde{y}_s + \dfrac{Q}{T_{Sv}^{max}}}, \tag{38′}$$

in the communication belt,

$$\tilde{\psi}_2^{lr} = \left(\frac{H_2}{H}\right)\frac{\alpha^{-1}\left(\tilde{y} - \tilde{y}_{cwbc}\right) + \left(\tilde{\psi}_b - \dfrac{Q}{T_{Sv}^{max}}\right)}{1 + \left(\dfrac{G_2}{\hat{F}}\right)} + \left(\frac{Q_2}{Q}\right)\left(\frac{Q}{T_{Sv}^{max}}\right)\frac{\alpha^{-1}\tilde{y}_{cwbc} + \dfrac{Q}{T_{Sv}^{max}}}{\alpha^{-1}\tilde{y}_s + \dfrac{Q}{T_{Sv}^{max}}} \tag{41′}$$

in the subtropical pool region, and

$$\tilde{\psi}_2^{lr} = \left(\frac{H_2}{H}\right)\frac{\alpha^{-1}\tilde{y} + \tilde{\psi}_b}{1 + \left(\dfrac{G_2}{\hat{F}}\right)}, \tag{42′}$$

in the subpolar pool region, and gives

$$\tilde{\psi}_2^{wbc} = \left[\left(\frac{Q_2}{Q}\right)\left(\frac{Q}{T_{Sv}^{max}}\right) - \tilde{\psi}_2^{lr}\left(\tilde{x} = 0\right)\right]\phi_{ys}(\tilde{y})\phi_m(\tilde{x}). \tag{34′}$$

In the communication belt, a new nondimensional parameter,

$$\frac{Q_2}{Q}, \tag{45}$$

is introduced to represent the ratio of the mass influx to the lower layer to the total mass influx to the moving layers. The lower layer transport through the communication belt is proportional to this ratio (or, more precisely, to Q_2/T_{Sv}^{max}).

The ψ_2^{lr} component in the pool regions further introduce two more nondimensional parameters, H_2/H and $\hat{F}/G_2 = \gamma_2 H/\gamma_1 H_1$. These two parameters represent the effect of the background stratification and also appear in the case without mass input, which has a nondimensional form as in (42′). In particular, the parameter $\hat{F}/G_2$ arises through the PV homogeneity approximation used in the pool regions.

The upper layer streamfunction is nondimensionalized by T_{Sv}^{max}/H_1 to yield

$$\tilde{\psi}_1 = \tilde{\psi}_b - \tilde{\psi}_2. \tag{21′}$$

4.4.2 Flow patterns within the lower and upper layers

Examples of $\tilde{\psi}_2$ and $\tilde{\psi}_1$ distributions are shown in Fig. 5 for cases (i) and (ii). The values of parameters are summarized in Table 1. The parameter Q_2 is set greater than Q ($Q_2/Q = 1.5$)*, to reflect the fact that downward diapycnal volume transport to the intermediate layer is induced by the convection in the Okhotsk Sea (NTIA06). The parameters H_2/H and $\hat{F}/G_2$ are set to 0.6 and 0.3, respectively, since these values lie within the parameter range of the NPIW.

When $Q = Q_2 = 0$, no inter-gyre flow occurs. This is due to the absence of both the communication belt and a

*The Oyashio water transport that contributes to the NPIW formation may give a rough estimate of Q_2, and is about 5–6 Sv (e.g., Shimizu *et al*., 2003). Although the Oyashio transport includes the influence of the Bering Sea, this may be regarded as mass input from the northwest corner, the effects of which are similar to that of the input from the western boundary. When $Q \sim 3$ Sv, Q_2/Q thus becomes about 2, whereas it is about 1 when $Q/T_{sv}^{max} = 0.2$ and $T_{sv}^{max} = 30$. We take the average of the two estimates for the value of Q_2/Q.

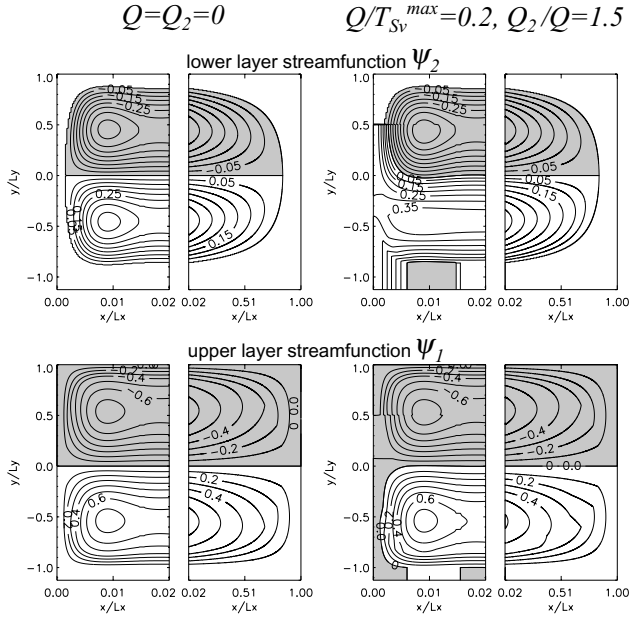

Fig. 5. (Top) Layer 2 streamfunction, ψ_2, and (bottom) layer 1 streamfunction, ψ_1. (Left) When $Q = Q_2 = 0$, (right) when $Q/T_{Sv}^{max} = 0.2$ and $Q_2/Q = 1.5$. ψ_2 and ψ_1 are nondimensionalized by T_{Sv}^{max}/H_2 and T_{Sv}^{max}/H_1, respectively. The contour interval is 0.05 for ψ_2 and 0.1 for ψ_1.

mass-driven western boundary current. Accordingly, the lower layer circulation is confined to the pool regions, and both $\tilde{\psi}_2$ and $\tilde{\psi}_1$ are symmetric about the gyre boundary.

In contrast, when $Q \neq 0$ and $Q_2 \neq 0$, the water supplied from the subpolar western boundary to the lower layer crosses the gyre boundary and moves toward the subtropics. This water separates from the western boundary and circulates in the interior. It then returns to the western boundary and eventually leaves the domain to enter the equatorial region. Overall, the flow path is similar to that of the NPIW and to the spreading route of the response to tidal mixing at the Kuril Straits, as implied by the impact on salinity distribution (NTIA06).

Distinct features are the inter-gyre transport near the western boundary and the entrainment into the interior. The former transport is considered to be important for NPIW formation (e.g., Talley, 1993; Yasuda *et al*., 1996), and is due to both the communication belt and the mass driven western boundary current in the lower layer, whereas the latter entrainment spreads water to an area that would be called the pool region in the absence of a net mass source (i.e., the communication belt and the pool region in the subtropics). Associated with the entrainment, the PV supplied from the mass source is carried through the communication belt and affects the PV value in the subtropical pool region.

In the subpolar region, the circulation in the pool region is scarcely changed in this solution since here the functional form of the solution becomes the same as that in the case without mass input. Although the model results in NTIA06 suggest that the streamfunction and PV values in the subpolar region are also modified, the QG approximation should be relaxed to express such an effect.

In contrast to the lower layer, the upper layer water flows from the equatorial to the subtropical regions through the western boundary current, and to the subpolar interior. The water then circulates along the outer rim of the subpolar gyre and leaves the domain by entering the mass sink, where the water is assumed to subduct into the lower layer.

4.4.3 Vertical structure of the inter-gyre flow

In the above case, the direction of the inter-gyre flow in the upper layer is opposite to that in the lower one. This kind of vertical structure in the inter-gyre transport through the western boundary region is determined by the ratio Q_2/Q in the present solution.

In the lower layer, the inter-gyre flow is equatorward when $Q_2 > 0$, absent when $Q_2 = 0$, and poleward when $Q_2 < 0$. This is because $\psi_2 = Q_2/H_2$ at $x = 0$ and for $y \leq y_s$ from (34). (Note that the equatorward flow corresponds to that away from the source and the poleward flow to that toward the sink.) In the upper layer, the direction of the inter-gyre flow is determined by Q_1 in the same manner, because $\psi_b = Q/H$ at $x = 0$ for $y \leq y_s$ from (17), and hence $\psi_1 = (Q - Q_2)/H_1 = Q_1/H_1$. Writing this condition in terms of Q_2 and Q, it follows that the upper layer inter-gyre flow is equatorward when $Q_2 < Q$, absent when $Q_2 = Q$, and poleward when $Q_2 > Q$.

Accordingly, the ratio Q_2/Q can be used to describe various combinations of upper and lower inter-gyre flow directions which determine the vertical structure of the western boundary current at the gyre boundary. When $Q > 0$, the following five cases can be considered (with flow paths shown in Appendix 2).

Case (1) when $Q_2/Q > 1$ ($Q_1 < 0$, $Q_2 > 0$): The inter-gyre flow is equatorward in the lower layer but poleward in the upper one. This is the case shown in the preceding sections.

Case (2) when $Q_2/Q = 1$ ($Q_1 = 0$, $Q_2 > 0$): The inter-gyre flow is equatorward in the lower layer but absent in the upper one. This situation could be realized when the convection from the upper to lower layer is either absent or compensated by upwelling from the lower to the upper layer.

Case (3) when $0 < Q_2/Q < 1$ ($Q_1 > 0$, $Q_2 > 0$): The inter-gyre flow is equatorward in both lower and upper layers. This situation occurs when the upwelling to the upper layer is larger than the convection to the lower layer

Table 2. Vertical structure for various Q_2/Q when $Q > 0$.

Case	Range	Lower layer flow	Upper layer flow
Case (1)	$Q_2/Q > 1$	equatorward	poleward
Case (2)	$Q_2/Q = 1$	equatorward	vanishes
Case (3)	$0 < Q_2/Q < 1$	equatorward	equatorward
Case (4)	$Q_2/Q = 0$	vanishes	equatorward
Case (5)	$Q_2/Q < 0$	poleward	equatorward

(i.e., the net mass flux is upward) and when this net mass flux to the upper layer is smaller than the upwelling from the abyssal layer.

Case (4) when $Q_2/Q = 0$ ($Q_1 > 0$, $Q_2 = 0$): The inter-gyre flow does not occur in the lower layer but is equatorward in the upper one. This situation occurs only when the upwelling to the upper layer exactly balances the sum of the upwelling and convection to the lower layer.

Case (5) when $Q_2/Q < 0$ ($Q_1 > 0$, $Q_2 < 0$): The inter-gyre flow is poleward in the lower layer but equatorward in the upper one. This situation occurs when the net mass flux between the upper and lower layers is upward and is larger than the upwelling from the abyssal layer.

The above cases are summarized in Table 2. The condition $Q < 0$ yields five similar cases, but the direction of the inter-gyre flow is opposite to those when $Q > 0$.

When $Q = 0$, both the lower and upper layer inter-gyre flows change their directions at $Q_2 = 0$, and hence the above five cases degenerate into three cases: $Q_2 = 0$ and $Q_2 \gtrless 0$. (Note that we should use Q_2 or a parameter proportional to Q_2 instead of Q_2/Q.) The case $Q_2 = 0$ corresponds to the wind-only scenario discussed in the previous section, into which the cases (2), (3) and (4) above degenerate. Here inter-gyre communication is minimal, either in terms of water circulation or geostrophic contours. The other two possibilities, $Q_2 > 0$ and $Q_2 < 0$, correspond to the cases (1) and (5) above, respectively. Interestingly, even if $Q = 0$, an inter-gyre flow does occur when $Q_2 \neq 0$, although geostrophic contours do not cross the gyre boundary. The flow paths for $Q = 0$ are also presented in Appendix 2.

5. Summary and Discussion

Although the key dynamical elements in the intermediate layer adjustment were identified as coastal Kelvin waves driven by mass input and eastward-advected long-Rossby waves in NTIA06, the effect of the adjustment through such Kelvin waves was not considered in ventilated thermocline theory, while that of the eastward moving long-Rossby waves within the wind-driven circulation has not been included in the abyssal circulation theory. As a first step to combine these two effects, we developed, in a rather heuristic manner, an idealized model of intermediate layer circulation and investigated the effects of mass input/output from the western boundary on the wind-driven circulation.

The model is a steady quasi-geostrophic (QG) 2.5-layer model. It is forced both by Ekman pumping, which produces subpolar and subtropical gyres, and by a mass source/sink, which feeds fluid from the subpolar western boundary at a rate Q_n into layer n with net mass input of $Q = Q_1 + Q_2$. A frictional western boundary layer is incorporated to represent the effect of Kelvin waves, which carry the mass away from the source, while the interior is approximated as inviscid and adiabatic.

The model describes the following ventilation process. Firstly, a net mass input induces a "barotropic" mode inter-gyre flow along the western boundary through the "Kelvin wave" dynamics. The "barotropic" inter-gyre flow then enables the geostrophic contours to make inter-gyre communication from the location of the mass source to the subtropical gyre. Some of these geostrophic contours turn eastward and extend into the interior owing to the effect of the wind-driven flow. These contours go around the outer rim of a zone that would represent the pool region in the absence of the mass input, and then return to the western boundary. Potential vorticity travels along the above path into the subtropical interior and affects the circulation. Eventually, the water supplied to the lower layer flows into the subtropics near the western boundary, circulates in the interior region along the above path, and then flows away toward the equatorial region. This is similar to the fate of the water ventilated in the Okhotsk Sea or the Kuril Straits. Conversely, in the upper layer, water is fed from the equator to subtropics, and to the subpolar interior through the western boundary current. The water then moves along the outer rim of the subpolar gyre and is absorbed into the mass sink (to be transformed around the Okhotsk Sea). In this way, the model illustrates a basic mechanism through which tidal mixing at the Kuril Straits and convection in the Okhotsk Sea ventilate the North Pacific intermediate layer.

The properties of the model are controlled by six nondimensional parameters, namely, Q/T_{Sv}^{max}, Q_2/Q, α, δ_m/L_x, H_2/H, and $G_2/\hat{F}$. The first two are introduced here, while the other four have been introduced in previous theories. Parameter Q/T_{Sv}^{max} is the ratio of net mass input rate to the maximum Sverdrup transport. This parameter determines the confluence point of "barotropic" western boundary currents (together with T_{Sv}^{min} or T_{Sv}^{ys} when $Q < 0$), and thus affects the inter-gyre communication through the western boundary layer by altering the paths of the geostrophic contours. Parameter Q_2/Q is the ratio of rate of mass input into the lower layer to that in all moving layers. This parameter determines the vertical structure of the western boundary current and controls the direc-

tion and volume transport of the inter-gyre flow in the upper and lower layers. Parameter α is a measure of the effect of wind forcing and determines the size of the pool region when $Q = 0$ (e.g., Pedlosky, 1996), and hence it determines the horizontal extent of the interior flow paths originating from the lower layer mass source in the present solution. The other parameter regimes with respect to $Q/T_{Sv}{}^{max}$ and Q_2/Q are presented in Appendices 1 and 2.

It should be noted that although the confluence point of the subtropical western boundary current is determined only by $Q/T_{Sv}{}^{max}$, Q_2/Q, and $Q/T_{Sv}{}^{min}$ (or $Q/T_{Sv}{}^{ys}$) in this model, a variety of other causative factors has been suggested in previous studies. Any slight shift of the separation point induced by these mechanisms would not significantly change the basic scenario, however. In addition, the result is not sensitive to the choice of a Munk or Stommel (1948) layer or to the use of a non-slip or slip condition, since these only modify the zonal structure function $\phi_m(x)$.

Although the present model assumes the input/output of mass leaks out of the model region, it is a matter for discussion whether the model agrees with the limiting case, in which the model region is closed and there are compensating mass source and sink at the western boundary in the model region. When the source is situated poleward of the sink, Kelvin waves carry the mass equatorward within the western boundary region from the source to the sink. The difference from the present model is the change in the meridional structure function, ϕ_{ys}, which now becomes

$$\begin{aligned} \phi_{ys}(y) &= 1, \quad \text{for } y_{sink} \le y \le y_s, \\ &= 0, \quad \text{for } y > y_s \ \text{ and } \ y < y_{sink}, \end{aligned} \tag{46}$$

where y_{sink} is the latitude of the sink.

On the other hand, when the sink is situated poleward of the source, Kelvin waves carry the mass around the basin counterclockwise in the northern hemisphere until the waves reach the sink. Rossby waves will then emanate from the eastern boundary to conduct an adjustment in the interior. As is shown in Subsection 3.1, the barotropic mass-driven flow should vanish in the interior in the present model configuration. However, input mass must be carried away from the western boundary region, otherwise the layer thickness there continues to increase. The present model resolves this problem by allowing the mass to leak out of the domain through the equatorward boundary. But for the closed basin, some processes neglected in the present model would be required. One possible solution may be the introduction of both a frictional boundary layer on the all closed boundaries and diapycnal mass transport from layer 2 to layer 3 in the model region. The former allows a flow along the boundaries, the

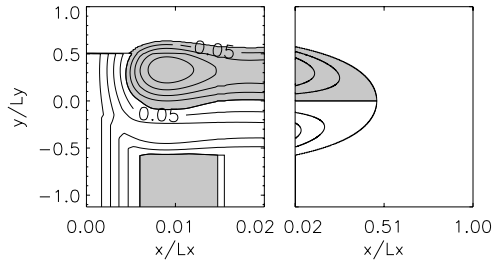

Fig. 6. Streamfunction in layer 2 in a parameter range corresponding to the deep western boundary current in the North Atlantic in the density range of the upper Labrador Sea Water. The parameter values are set, following Spall (1996), as $Q/T_{Sv}{}^{max} = 10/41$, $Q_2/Q = 1$, $\alpha = 0.6$, $H_2/H = 900/1750$, and $G_2/\hat{F} = 0.06$. The other settings are the same as those in Fig. 5.

southern boundary in particular, and the latter allows the damping Rossby waves propagating from the eastern boundary (in other words, non-zero $\psi_b{}^m$ is possible in the interior owing to the diapycnal transport). The situation then becomes similar to the lower layer of Kawase's (1987) model. Note that, different from the present model, the interior dynamics is not Sverdrupian in such a case. The extension to such a model is left for future work.

Within a certain parameter range, the model shows some similarities to the results of the numerical experiments of Spall (1996) and Katsman *et al.* (2001) (Fig. 6). For example, the lower layer flow originating from the mass source is split into two mean paths, one moving to the equator along the western boundary and the other into the interior. The interior path merges with the other path along the boundary after circulating within the interior. This feature is also similar to the observed deep western boundary current (DWBC) in the density range of the upper Labrador Sea Water (e.g., Talley and McCartney, 1982; Pickart and Smethie, 1993; Bower and Hunt, 2000). Spall (1996) also showed that the presence of the DWBC does not preclude the formation of a large region of homogenized PV, but that it does affect the interior value of PV. In addition, the horizontal extent of the interior path increases as the Gulf Stream or wind forcing is enhanced. These three features are consistent with the following three features of the present model, respectively: the approximation of PV homogeneity, the transport of PV from the mass source to the subtropical interior along the geostrophic contours, and the fact that the interior flow path lies along the communication belt and hence its horizontal extent is controlled by the parameter α. These similarities exist between our steady and rather simple model and the numerical results, despite the fact that Spall (1996) used an eddy-permitting primitive model. The present model is therefore expected to incorporate the essential

physics required to understand intermediate layer ventilation and thus we hope that the model may provide an insight useful for the construction of a theory of ventilation from the ventilated thermocline to the abyss.

Acknowledgements

We wish to acknowledge Dr. J. P. Matthews for his critical reading. The first author thanks Dr. H. Mitsudera for his encouraging comment. Thanks are extended to the reviewers for their useful comments. The comment of Reviewer 1 is particularly helpful to improve the solution of ψ_2^{lr}. This study was supported by the Category 7 of MEXT RR2002 Project for Sustainable Coexistence of Human, Nature and the Earth and by a Grant-in-Aid for the 21st Century COE Program (Kyoto University, G3). T.N. was partly supported by the JSPS Research Fellowships for Young Scientists and by a Grant-in-Aid for Young Scientists.

Appendix 1: Barotropic Flow and Geostrophic Contours for Various Q/T_{Sv}^{max}

Changes in the paths of the "barotropic" flow and geostrophic contours from the case $Q/T_{Sv}^{max} = 0$ to $Q/T_{Sv}^{max} = 0.2$ are discussed in Subsection 3.2. Here, path changes resulting from variation in the Q/T_{Sv}^{max} parameter are discussed. Figure A1 shows maps of ψ_b and $\hat{q}_2$ for various values of Q/T_{Sv}^{max}. The other settings are the same as those in Fig. 4.

Noticeable path changes for ψ_b and $\hat{q}_2$ take place at $Q/T_{Sv}^{max} = 0$, 1, and $T_{Sv}^{min}/T_{Sv}^{max}$ (or T_{Sv}^{ys}/T_{Sv}^{max}) associated with the shift of y_{cwbc}, the confluence point of the western boundary currents in the subpolar and subtropical gyres discussed in Subsection 3.2.1. The paths are thus characterized into seven types when the three cases of $Q/T_{Sv}^{max} = 0$, 1, and $T_{Sv}^{min}/T_{Sv}^{max}$ are considered separately. For simplicity, the case $T_{Sv}^{min} = T_{Sv}^{ys}$ (i.e., $y_{cspg} = y_s$) is presented here. Note also that $T_{Sv}^{min}/T_{Sv}^{max} = -1$ in all the cases presented here, since $T_{Sv}^{min} = -T_{Sv}^{max}$ from (19).

Type (i) when $Q/T_{Sv}^{max} = 0$ (i.e., no net mass input/output). The circulation is driven only by wind, and there is no inter-gyre transport for the barotropic mode, as discussed in Section 3 (Fig. 4).

Type (ii) when $0 < Q/T_{Sv}^{max} < 1$ (i.e., a moderate mass input). The confluence y_{cwbc} is in the subtropical gyre, so that "barotropic" inter-gyre transport occurs and that the communication belt appears, as described in Subsection 4.2. Variations in this range are given from (18), (17), and (33), which indicate that an increase in Q/T_{Sv}^{max} causes an equatorward shift of y_{cwbc} from the gyre boundary toward the center of the subtropical gyre, an increase in volume transport of the barotropic inter-gyre flow, broadening of the communication belt, and shrinking of the subtropical pool region.

Type (iii) when $Q/T_{Sv}^{max} = 1$ (i.e., the mass input rate equals the maximum Sverdrup transport in the subtropical gyre). The poleward western boundary current vanishes, and the Sverdrup flow into the subtropical interior is compensated solely by mass input from the western boundary. This results in the absence of both a closed barotropic streamline and a pool region in the subtropical gyre.

Type (iv) when $Q/T_{Sv}^{max} > 1$ (i.e., a large mass input). An equatorward western boundary current flows through the subtropics. The streamlines from the mass source diverge to form both this boundary current and a flow circulating in the interior. They later converge to flow into the equatorial region.

Type (v) when $T_{Sv}^{min}/T_{Sv}^{max} < Q/T_{Sv}^{max} < 0$ (i.e., a moderate mass output). The confluence y_{cwbc} is in the subpolar gyre. Interestingly, the "barotropic" cross-gyre transport flows from the equatorial region through the subtropical western boundary current to the subpolar interior, circulates around the outer rim of the subpolar gyre, and eventually flows into the mass sink. Associated with this, geostrophic contours originating from the subtropical eastern boundary and/or the equatorial region extend through the subtropical western boundary current to the subpolar interior. These contours correspond to a subpolar counterpart of the communication belt discussed in Subsection 4.2. Associated with this subpolar communication belt, shrinkage takes place in the subpolar pool region rather than the subtropical pool.

Variations in this range are similar to those in the case $Q > 0$. An increase in $|Q/T_{Sv}^{max}|$ causes a poleward shift of y_{cwbc} from the gyre boundary toward the mass sink, an increase in volume transport of the barotropic inter-gyre flow, broadening of the subpolar communication belt and shrinkage of the subpolar pool region.

Type (vi) when $Q/T_{Sv}^{max} = T_{Sv}^{min}/T_{Sv}^{max}$ (i.e., the mass output rate equals to the minimum Sverdrup transport at the western boundary). In contrast to the case $Q/T_{Sv}^{max} = 1$, the subpolar western boundary current vanishes only on the equator side of y_s because of the Kelvin wave dynamics. In addition, both closed streamlines and the pool region remain in the subpolar gyre on the poleward side of y_s. This is due to the oscillatory structure of the Munk layer. It should be noted that when $y_s < y_{cspg}$ and $Q = T_{Sv}^{ys}$, such closed paths are present even for the Stommel layer. Accordingly, when $Q < 0$, both the latitudinal position of the mass sink and the longitudinal structure of the western boundary current affect the subpolar gyre circulation.

Type (vii) when $Q/T_{Sv}^{max} < T_{Sv}^{min}/T_{Sv}^{max}$ (i.e., a large mass output). The streamlines extending from the equatorial region diverge to form the poleward, subpolar western boundary current and a flow circulating within the subpolar interior. They later converge to flow into the mass sink.

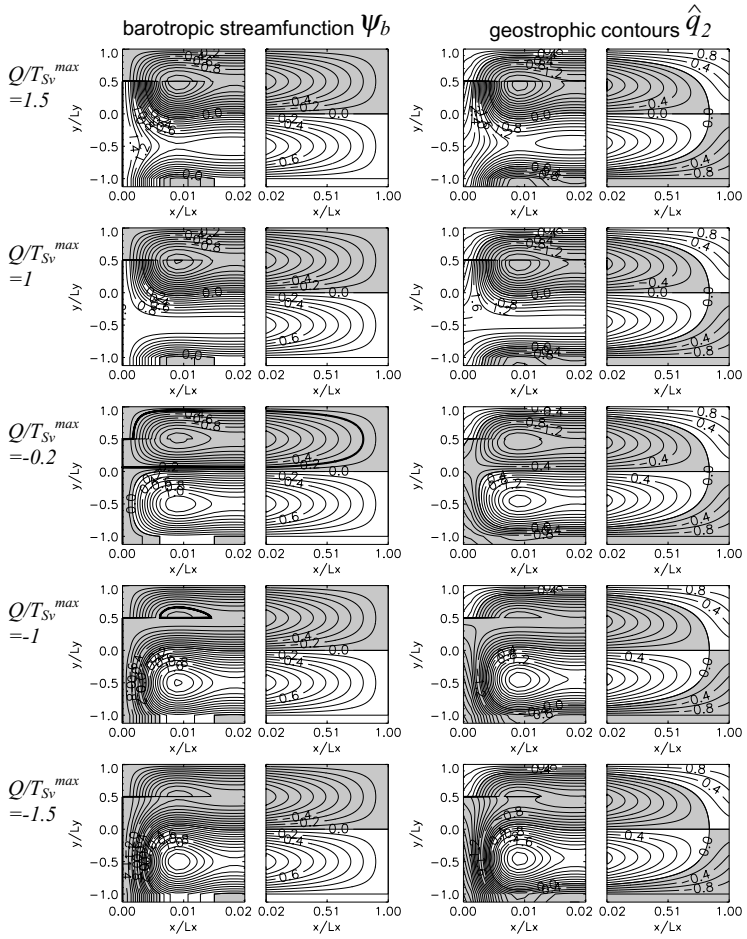

Fig. A1. (Left) Barotropic mode streamfunction and (right) geostrophic contours for various values of Q/T_{Sv}^{max}, which are selected so that the seven types discussed in Appendix 1 are represented (the cases $0 < Q/T_{Sv}^{max} < 1$ and $Q/T_{Sv}^{max} = 0$ are shown in Fig. 4). The other settings are the same as those in Fig. 4.

Appendix 2: Upper and Lower Layer Streamfunctions for Various Q_2/Q

Flow paths of the "baroclinic" mode for various Q_2/Q are shown in Fig. A2. The baroclinic-flow paths change as the vertical structure of the western boundary current changes, which is categorized into the five cases (Table 2). The values of Q_2 are selected to represent these cases.

The values of Q are set as $0.2T_{Sv}^{max}$ and 0, which represent the two barotropic flow types considered in Sections 3 and 4 (i.e., those when $0 < Q/T_{Sv}^{max} < 1$ and $Q = 0$). The other regimes are omitted for the following reasons. When $Q \geq 1$, streamlines exhibit interesting features associated with the absence of the subtropical pool region (the corresponding region is occupied by the communication belt) and with the presence of a flow from the mass source to the equatorial region along the western boundary (or from the equatorial region to the sink). This regime is omitted, however, because it rarely occurs in major basins. When $Q < 0$, geostrophic contours emanating from the western equatorial region are present (Appendix 1), so that an additional boundary condition on the equator side of the subtropical gyre is required to obtain a solution. Since such a condition depends on the situations in the western equatorial regions, which differ considerably between basins, we do not include this regime in the figure.

A2.1 $0 < Q/T_{Sv}^{max} < 1$

When $Q > 0$, the lower layer circulation changes at $Q_2/Q = 0$ as the lower layer inter-gyre flow changes its direction, while that in the upper layer changes at $Q_2/Q = 1$. We thus describe the circulation in these two layers separately.

The lower layer inter-gyre flow is equatorward, when $Q_2/Q > 0$. This includes the case shown in Subsection 4.4.2. The water fed from the mass source flows away through the subpolar western boundary region to the subtropical interior, and to the equatorial western boundary

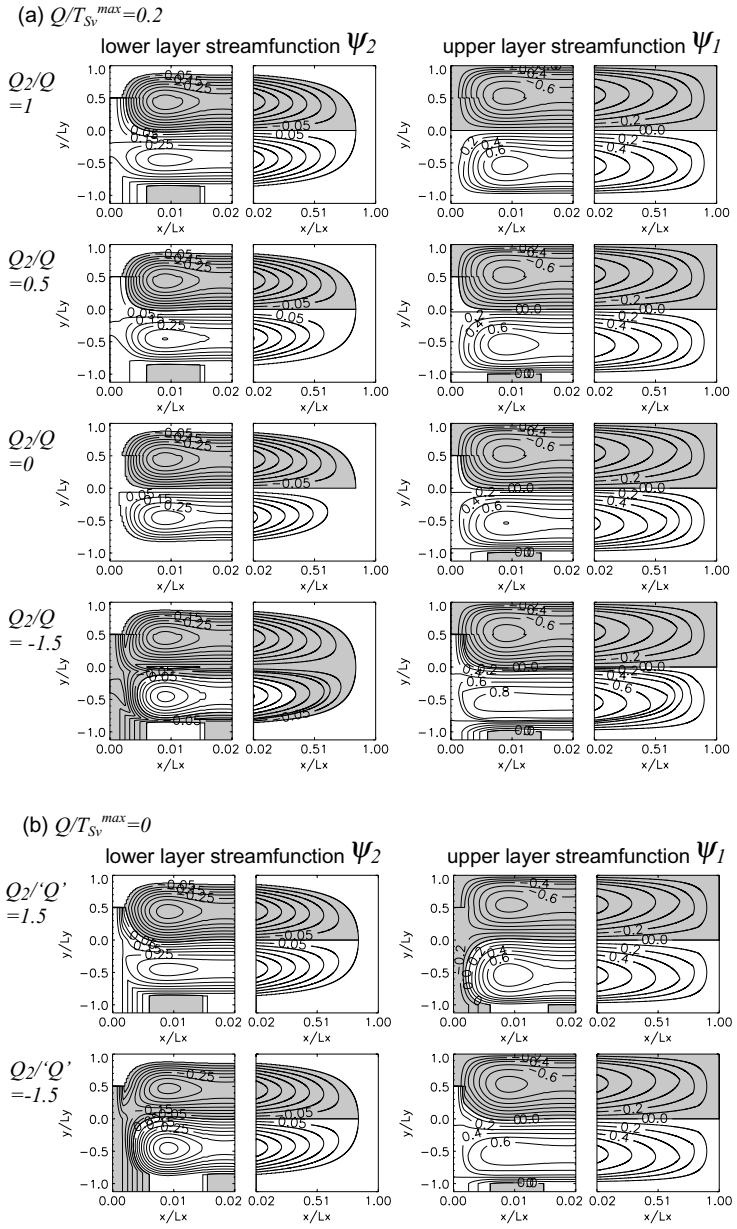

Fig. A2. Streamfunctions of (left) the lower and (right) upper layers for various values of Q_2/Q, when (a) Q/T_{Sv}^{max} = 0.2 and (b) Q/T_{Sv}^{max} = 0. In the case (b), Q_2 is normalized by "Q", which is the value of Q in the case (a), in order to facilitate the comparison. The other settings are the same as those in Fig. 5.

region. Although such qualitative features remain the same in this range, the inter-gyre transport increases with increasing Q_2/Q.

When $Q_2/Q = 0$, the lower layer inter-gyre flow vanishes. This is because the absence of a mass input in the lower layer works to restrict the flow in the communication belt. Thus, in terms of water circulation, inter-gyre communication vanishes in the lower layer, although the information travels through the communication belt. The subtropical pool region is still in motion, but the PV value is different from that in the wind only case. When $Q/T_{Sv}^{max} \geq 1$, the whole subtropical gyre becomes stagnant in the lower layer as the subtropical pool region disappears.

When $Q_2/Q < 0$, the lower layer inter-gyre flow is directed poleward to the mass sink: Water flows from the equatorial region to the subtropics, splits into two paths (one along the western boundary and one encircling the subtropical interior), enters the subpolar western boundary region, and finally flows into the mass sink.

The upper layer inter-gyre flow is poleward, when $Q_2/Q > 1$, which is the case shown in Fig. 5. The water crossing gyre boundaries flows from the equatorial region to the subtropics through the western boundary region, and to the subpolar interior (the outer rim of the subpolar gyre). This flow path is similar to that of the barotropic mode in the case $Q/T_{Sv}{}^{max} < 0$, rather than that of the lower layer in the case $Q_2/Q < 0$.

When $Q_2/Q = 1$, the upper layer inter-gyre flow vanishes. Thus, all of the mass input from the western boundary is transported through the lower layer.

When $Q_2/Q < 1$, the upper layer inter-gyre flow is directed equatorward. As a result, the input water flows from the subpolar western boundary region into the outer rim of the subtropical gyre, and to the equatorial region.

A2.2 $Q = 0$

When $Q = 0$, both the lower and upper layer circulation paths change at $Q_2 = 0$, as the inter-gyre flows in both layers change their directions. When $Q_2 > 0$, the inter-gyre flow is equatorward in the lower layer but poleward in the upper one. Thus, the water fed into the lower layer flows from the subpolar region to the subtropics, and to the equator, similar to the cases when $Q > 0$ and $0 < Q_2/Q < 1$. Conversely, in the upper layer, the water coming from the equatorial region flows through the subtropics to the subpolar gyre, similar to when $Q > 0$ and $Q_2/Q > 1$.

When $Q_2 < 0$, the inter-gyre flow in both layers reverses its direction (i.e., it becomes poleward in the lower layer and equatorward in the upper layer). Associated with this, the lower layer circulation becomes similar to the case when $Q > 0$ and $Q_2/Q < 0$, while the upper layer flow is similar to when $Q > 0$ and $Q_2/Q < 1$.

It should be noted that because geostrophic contours in the interior are not affected by mass input/output, the flow paths in the interior region remain the same in the present model, even though an inter-gyre flow is induced by the mass input/output.

References

Alfultis, M. A. and S. Martin (1987): Satellite passive microwave studies of the Sea of Okhotsk Sea ice cover and its relation to oceanic processes. *J. Geophys. Res.*, **92**, 13,013–13,028.

Aoki, K. and K. Kutsuwada (2008): Verification of the wind-driven transport in the North Pacific subtropical gyre using gridded wind-stress products. *J. Oceanogr.*, **64**, 49–60.

Aramaki, T., S. Watanabe, T. Kuji and M. Wakatsuchi (2001): The Okhotsk-Pacific seawater exchange in the viewpoint of vertical profiles of radiocarbon around the Bussol' Strait. *Geophys. Res. Lett.*, **28**, 3971–3974.

Bower, A. S. and H. D. Hunt (2000): Lagrangian observations of the deep western boundary current in the North Atlantic Ocean. Part I: Large-scale pathways and spreading rates. *J. Phys. Oceanogr.*, **30**, 764–783.

Cember, R. P. (1998): On deep western boundary currents. *J. Geophys. Res.*, **103**, 5397–5417.

Chen, L. G. and W. K. Dewar (1993): Intergyre communication in a three-layer model. *J. Phys. Oceanogr.*, **23**, 855–878.

Edwards, C. A. and J. Pedlosky (1995): The influence of distributed sources and upwelling on the baroclinic structure of the abyssal circulation. *J. Phys. Oceanogr.*, **25**, 2259–2284.

Ffield, A. and A. L. Gordon (1992): Vertical mixing in the Indonesian thermocline. *J. Phys. Oceanogr.*, **22**, 184–195.

Gladyshev, S. V. (1995): Fronts in the Kuril Island region. *Oceanology*, English translation, **34**, 452–459.

Hautala, S. L. and S. C. Riser (1989): A simple model of abyssal circulation, including effects of wind, buoyancy and topography. *J. Phys. Oceanogr.*, **19**, 596–611.

Hogg, N. G. and H. Stommel (1985): On the relation between the deep circulation and the Gulf Stream. *Deep-Sea Res.*, **32**, 1181–1193.

Huang, R. X. (1990): Matching a ventilated thermocline model with inertial western boundary currents. *J. Phys. Oceanogr.*, **20**, 1599–1607.

Huang, R. X. and G. R. Flierl (1987): Two-layer models for the thermocline and current structure in subtropical/subpolar gyres. *J. Phys. Oceanogr.*, **17**, 872–884.

Ishizaki, H. (1994): A simulation of the abyssal circulation in the North Pacific Ocean. Part II: Theoretical rationale. *J. Phys. Oceanogr.*, **24**, 1941–1954.

Jarvis, R. A. and G. Veronis (1994): Strong deep recirculation in a two-layer wind-driven ocean. *J. Phys. Oceanogr.*, **24**, 759–776.

Katsman, C. A., S. S. Drifhout and H. A. Dijkstra (2001): The interaction of a deep western boundary current and the wind-driven gyres as a cause for low-frequency variability. *J. Phys. Oceanogr.*, **31**, 2321–2339.

Kawasaki, Y. and T. Kono (1994): Distribution and transport of Subarctic Waters around the middle of Kuril Islands. *Sea and Sky*, **70**, 71–84 (in Japanese with English abstract and figure captions).

Kawase, M. (1987): Establishment of deep ocean circulation driven by deep-water production. *J. Phys. Oceanogr.*, **17**, 2294–2317.

Kitani, K. (1973): An oceanographic study of the Okhotsk Sea—particularly in regard to cold waters. *Bull. Far Seas Fish. Res. Lab.*, **9**, 45–77.

Liu, Z., L. Wu and E. Bayler (1999): Rossby wave-coastal Kelvin wave interaction in the extratropics. Part I: Low-frequency adjustment in a closed basin. *J. Phys. Oceanogr.*, **29**, 2382–2404.

Lukas, R., E. Firing, P. Hacker, P. L. Richardson, C. A. Collins, F. Fine and R. Gammon (1991): Observations of the Mindanao Current during the Western Equatorial Pacific Ocean Circulation Study. *J. Geophys. Res.*, **96**, 7089–7104.

Luyten, J. R. and H. M. Stommel (1986): Experiments with cross-gyre flow patterns on a beta-plane. *Deep-Sea Res.*, **33**, 963–972.

Luyten, J. R., J. Pedlosky and H. Stommel (1983): The ventilated thermocline. *J. Phys. Oceanogr.*, **13**, 292–309.

Mitsudera, H., B. Taguchi, Y. Yoshikawa, H. Nakamura, T. Waseda and T. D. Qu (2004): Numerical study on the

Oyashio water pathways in the Kuroshio-Oyashio confluence. *J. Phys. Oceanogr.*, **34**, 1174–1196.
Munk, W. H. (1950): On the wind-driven ocean circulation. *J. Meteor.*, **7**, 79–93.
Nakamura, T. and T. Awaji (2001): A growth mechanism for topographic internal waves generated by an oscillatory flow. *J. Phys. Oceanogr.*, **31**, 2511–2524.
Nakamura, T. and T. Awaji (2004): Tidally induced diapycnal mixing in the Kuril Straits and the roles on water transformation and transport processes: A three-dimensional nonhydrostatic model experiment. *J. Geophys. Res.*, **109**, doi:10.1029/2003JC001850.
Nakamura, T., T. Awaji, T. Hatayama, K. Akitomo, T. Takizawa, T. Kono, Y. Kawasaki and M. Fukasawa (2000): The generation of large-amplitude unsteady lee waves by subinertial K_1 tidal flow: a possible vertical mixing mechanism in the Kuril Straits. *J. Phys. Oceanogr.*, **30**, 1601–1621.
Nakamura, T., T. Toyoda, Y. Ishikawa and T. Awaji (2004): Tidal mixing in the Kuril Straits and its impact on ventilation in the North Pacific Ocean. *J. Oceanogr.*, **60**, 411–423.
Nakamura, T., T. Toyoda, Y. Ishikawa and T. Awaji (2006a): Enhanced ventilation in the Okhotsk Sea through tidal mixing at the Kuril Straits. *Deep Sea Res. I*, **53**, 425–448.
Nakamura, T., T. Toyoda, Y. Ishikawa and T. Awaji (2006b): Effects of tidal mixing at the Kuril Straits on North Pacific ventilation: Adjustment of the intermediate layer revealed from numerical experiments. *J. Geophys. Res.*, **109**, C04003, doi:10.1029/2005JC003142.
Pedlosky, J. (1984): Cross-gyre ventilation of the subtropical gyre: An internal mode in the ventilated thermocline. *J. Phys. Oceanogr.*, **14**, 1172–1178.
Pedlosky, J. (1987): *Geophysical Fluid Dynamics*. 2nd ed., Springer-Verlag Inc., New York, 710 pp.
Pedlosky, J. (1992): The baroclinic structure of the abyssal circulation. *J. Phys. Oceanogr.*, **22**, 652–659.
Pedlosky, J. (1996): *Ocean Circulation Theory*. Springer-Verlag Inc., Berlin, Heidelberg, 453 pp.
Pedlosky, J. and D. C. Chapman (1993): Baroclinic structure of the abyssal circulation and the role of meridional topography. *J. Phys. Oceanogr.*, **23**, 979–991.
Pickart, R. S. and W. M. Smethie, Jr. (1993): How does the deep western boundary current cross the Gulf Stream? *J. Phys. Oceanogr.*, **23**, 2602–2616.
Rhines, P. B. and W. R. Young (1982): A theory of the wind-driven circulation I. Mid-Ocean Gyres. *J. Mar. Res.*, **40** (Supp.), 559–596.
Schopp, R. (1988): Spinup toward communication between large oceanic subpolar and subtropical gyres. *J. Phys. Oceanogr.*, **18**, 1241–1259.
Schopp, R. (1993): Multiple equilibria for cross-gyre flow between subpolar and subtropical gyres. *J. Phys. Oceanogr.*, **23**, 1754–1766.
Schopp, R. and M. Arhan (1986): A ventilated middepth circulation model for the eastern North Atlantic. *J. Phys. Oceanogr.*, **16**, 344–357.
Shimizu, Y., I. Yasuda, K. Okuda, K. Hanawa and S-I. Ito (2003): ADCP-referenced Kuroshio and Oyashio water transports for North Pacific Intermediate Water formation. *J. Phys. Oceanogr.*, **33**, 220–233.
Spall, M. A. (1996): Dynamics of the Gulf Stream/Deep Western Boundary Current cross over. Part I: Entrainment and recirculation. *J. Phys. Oceanogr.*, **26**, 2152–2168.
Speer, K. G. and M. S. McCartney (1992): Bottom water circulation in the western North Atlantic. *J. Phys. Oceanogr.*, **22**, 83–92.
Stommel, H. (1948): The westward intensification of wind-driven ocean currents. *Trans. Am. Geophys. Union*, **29**, 202–206.
Stommel, H., and A. B. Arons (1960): On the abyssal circulation of the world ocean, II An idealized model of the circulation pattern and amplitude in oceanic basins. *Deep-Sea Res.*, **6**, 217–233.
Straub, D. N. and P. B. Rhines (1990): Effects of large-scale topography on abyssal circulation. *J. Mar. Res.*, **48**, 223–253.
Straub, D. N., P. D. Killworth and M. Kawase (1993): A simple model of mass-driven abyssal circulation over a general bottom topography. *J. Phys. Oceanogr.*, **23**, 1454–1469.
Talley, L. D. (1991): An Okhotsk Sea water anomaly: implications for ventilation in the North Pacific. *Deep-Sea Res.*, **38**, S171–S190.
Talley, L. D. (1993): Distribution and formation of North Pacific Intermediate Water. *J. Phys. Oceanogr.*, **23**, 517–537.
Talley, L. D. and M. S. McCartney (1982): Distribution and circulation of Labrador Sea Water. *J. Phys. Oceanogr.*, **12**, 1189–1205.
Tatebe, H. and I. Yasuda (2004): Oyashio southward intrusion and cross-gyre transport related to diapycnal upwelling in the Okhotsk Sea. *J. Phys. Oceanogr.*, **34**, 2327–2341.
Warner, M. J., J. L. Bullister, D. P. Wisegraver, R. H. Gammon and R. F. Weiss (1996): Basin-wide distributions of chlorofluorocarbons CFC-11 and CFC-12 in the North Pacific. *J. Geophys. Res.*, **101**, 20,525–20,542.
Watanabe, Y. W., K. Harada and K. Ishikawa (1994): Chlorofluorocarbons in the central North Pacific and southward spreading time of North Pacific intermediate water. *J. Geophys. Res.*, **99**, 25,195–25,213.
Wong, C. S., R. J. Matear, H. J. Freeland, F. A. Whitney and A. S. Bychkov (1998): WOCE line P1W in the Sea of Okhotsk 2. CFCs and the formation rate of intermediate water. *J. Geophys. Res.*, **103**, 15,625–15,642.
Yamanaka, G., Y. Kitamura and M. Endoh (1998): Formation of North Pacific Intermediate Water in Meteorological Research Institute ocean general circulation model, 1. Subgrid-scale mixing and marginal sea fresh water. *J. Geophys. Res.*, **103**, 30,885–30,903.
Yamanaka, Y. and E. Tajika (1996): The role of the vertical fluxes of particulate organic matter and calcite in the oceanic carbon cycle: Studies using biogeochemical general circulation model. *Global Biogeochem. Cycles*, **10**, 361–382.
Yasuda, I., K. Okuda and Y. Shimizu (1996): Distribution and formation of North Pacific Intermediate Water in the Kuroshio-Oyashio interfrontal zone. *J. Phys. Oceanogr.*, **26**, 448–465.
Yasuoka, T. (1968): Hydrography in the Okhotsk Sea—(2). *The Oceanographical Magazine*, **20**, 55–63.
Young, W. R. and P. B. Rhines (1982): A theory of the wind-driven circulation II. Gyres with western boundary layers. *J. Mar. Res.*, **40**, 849–872.